blood®
Regular Article

LYMPHOID NEOPLASIA

BTG1 inactivation drives lymphomagenesis and promotes lymphoma dissemination through activation of BCAR1

Lorric Delage,[1,2] Mireille Lambert,[3] Émilie Bardel,[1,2] Cindy Kundlacz,[4] Dimitri Chartoire,[1,2] Axel Conchon,[1,2] Anne-Laure Peugnet,[1,2] Lucas Gorka,[2] Patrick Auberger,[5] Arnaud Jacquel,[5] Carole Soussain,[6] Olivier Destaing,[7] Henri-Jacques Delecluse,[8] Susanne Delecluse,[8] Samir Merabet,[4] Alexandra Traverse-Glehen,[1,2] Gilles Salles,[9] Emmanuel Bachy,[1,2] Marc Billaud,[10] Hervé Ghesquières,[1,2] Laurent Genestier,[1,2] Jean-Pierre Rouault,[2,10,*] and Pierre Sujobert[1,2,*]

[1]Centre International de Recherche en Infectiologie (Team LIB), Université Lyon, INSERM, U1111, Université Claude Bernard Lyon 1, Centre National de la Recherche Scientifique, UMR5308, ENS de Lyon, Lyon, France; [2]Faculté de Médecine Lyon-Sud, Université de Lyon, Oullins, France; [3]Université de Paris, Institut Cochin, INSERM U1016, Plateforme BioMecan'IC, Biomécanique de la cellule, Paris, France; [4]Institut de Génomique Fonctionnelle de Lyon, Centre National de la Recherche Scientifique UMR5242, Université Lyon 1, Ecole Normale Supérieure de Lyon, Lyon, France; [5]Université Côte d'Azur, Centre Méditerranéen de Médecine Moléculaire (C3M), INSERM U1065, Nice, France; [6]Institut Curie, Site de Saint-Cloud, Hematologie, et INSERM U932 Institut Curie, PSL Research University, Paris, France; [7]Centre de Recherche UGA, INSERM U1209, Institute for Advanced Biosciences, Grenoble, France; [8]German Cancer Research Center, Heidelberg, Germany; [9]Memorial Sloan Kettering Cancer Center, New York, NY; and [10]INSERM Unité Mixte de Recherche (UMR)-U1052, Centre National de la Recherche UMR 5286, Centre de Recherche en Cancérologie de Lyon, Lyon, France

KEY POINTS

- **BTG1 inactivation drives lymphomagenesis.**
- **BTG1 inactivation promotes lymphoma dissemination through the BCAR1-RAC1 pathway, which is targetable by dasatinib.**

Understanding the functional role of mutated genes in cancer is required to translate the findings of cancer genomics into therapeutic improvement. *BTG1* is recurrently mutated in the MCD/C5 subtype of diffuse large B-cell lymphoma (DLBCL), which is associated with extranodal dissemination. Here, we provide evidence that *Btg1* knock out accelerates the development of a lethal lymphoproliferative disease driven by Bcl2 overexpression. Furthermore, we show that the scaffolding protein BCAR1 is a BTG1 partner. Moreover, after *BTG1* deletion or expression of *BTG1* mutations observed in patients with DLBCL, the overactivation of the BCAR1-RAC1 pathway confers increased migration ability in vitro and in vivo. These modifications are targetable with the SRC inhibitor dasatinib, which opens novel therapeutic opportunities in *BTG1* mutated DLBCL.

Introduction

Diffuse large B-cell lymphoma (DLBCL) is the most common subtype of lymphoma. Approximately two-thirds of patients with DLBCL can be cured with intensive immunochemotherapy, but this disease remains an unmet medical need for unfit patients or patients with relapse/refractory disease.[1] Following the description of the transcriptomic heterogeneity of DLBCL,[2] functional analysis of the activated B cell (ABC) and germinal center (GC) subtypes have revealed specific targetable oncogenic addictions[3] and synthetic lethal interactions.[4] However, randomized clinical trials based on these preclinical data have failed to demonstrate a measurable clinical benefit of adding drugs to immunochemotherapy backbones.[5-7] An interesting explanation of these disappointing clinical results comes from genomic studies, which have revealed a more complex classification of DLBCL based on genomic subgroups of clinical significance.[8-10] Among these subgroups, the MCD/C5 subtype, characterized by *MYD88* and *CD79B* mutations with an ABC transcriptomic profile, is associated with extranodal dissemination, and very poor prognosis. This subtype is also associated with recurrent mutations in other genes, such as *TBL1XR1*[11] or *BTG1* (40% of patients).

BTG1 is a highly conserved gene, a prototype of the BTG-TOB antiproliferative gene family.[12-15] *BTG1* is a bona fide tumor suppressor gene in pediatric B-cell precursor acute lymphoblastic leukemia, in which deletions are observed in 10% of patients, and have been associated with corticosteroid resistance.[16,17] The functions of this gene remain elusive except for its interactions with the messenger RNA deadenylation complex CCR4-Not[18,19] and with the arginine methyl transferase PRMT1.[20,21] In lymphomas, *BTG1* mutations are missense (85%) or nonsense with no mutational hotspot. As *BTG1* mutations harbor the signature of activation-induced cytidine deaminase,[22] they were often considered as passengers in lymphomagenesis.[23] However, the specific enrichment of *BTG1* mutations in the MCD/C5 subtype of DLBCL and the poor prognostic value conferred by BTG1 mutations in ABC-DLBCL[24] raises the alternative hypothesis that they actively contribute to

lymphomagenesis, which is also supported by recent genomic analysis.[25]

The objective of this study was to experimentally assess the role of BTG1 in lymphomagenesis, and to assess the functional consequences of *BTG1* inactivation, especially regarding the frequency of extranodal dissemination observed in *BTG1*-mutated DLBCL.

Methods

Cell lines

The DLBCL cell lines TMD8[26] (RRID:CVCL_A442), SUDHL-4 (ATCC Cat# CRL-2957, RRID:CVCL_0539), and OCI-Ly10 (RRID:CVCL_8795) containing Cas9 protein were generated by transduction with lentiCas9-blast virus (Addgene #125592, Watertown, MA), and selected with 2.5 μg/mL blasticidin for 7 days. TMD8 and SUDHL-4 cells were grown in Roswell Park Memorial Institute 1640 GlutaMAX supplement medium (12027599; Thermo Fisher Scientific, Waltham, MA), supplemented with 10% fetal calf serum (FCS, CVFSVF0001; Eurobio, Evry, France) and 1% penicillin G/streptomycin (5000 U/mL). OCI-Ly10 cells were grown in Iscove modified Dulbecco, GlutaMAX supplement medium (IMDM, 31980030, Thermo Fisher Scientific, Waltham, MA), supplemented with 20% FCS (CVFSVF0001, Eurobio, Evry, France) and 1% penicillin G/streptomycin (5000 U/mL). HEK293T cells (ATCC Cat# CRL-3216, RRID:CVCL_0063) were maintained in Dulbecco's modified Eagle medium (11965092; Thermo Fisher Scientific, Waltham, MA) supplemented with 10% FCS and 1% penicillin G/streptomycin (15140122; Thermo Fisher Scientific, Waltham, MA). All cells were grown in incubators at 37°C, in a 5% CO_2 atmosphere. (Specific information are available in supplemental Methods, available on the *Blood* website)

Murine models

Generation of *BTG1*$^{-/-}$ and VavP-BCL2 mice have been described previously.[27,28] VaVP-BCL2 mice were kindly provided by Jerry Adams (WEHI, Victoria, Australia). C57BL/6J wild-type (WT) (RRID:IMSR_JAX:000664) and NOD.Cg-*Prkdc*^{scid}*Il2rg*^{tm1Wjl}/SzJ (NSG) (RRID:IMSR_JAX:005557) mice were purchased from Charles River laboratory (St-Germain sur l'Arbresle, France). All mice were maintained under pathogen-free conditions at the Plateau de Biologie Expérimentale de la Souris (Ecole Normale Supérieure de Lyon, France). All studies and procedures were performed in accordance with European Union guidelines and were approved by the local animal ethics evaluation committee (APAFIS 20171129160482).

Bone marrow transplantation

Bone marrow cells of VavP-BCL2-Btg1$^{-/-}$ and VavP-BCL2-Btg1^{WT} mice were harvested from the tibia and femur of 8- to 12-week-old donor mice. After treatment with red blood cell lysis buffer ACK solution (Thermo Fisher Scientific, Waltham, MA), 3 million cells were injected retro-orbitally into lethally irradiated C57BL/6J host mice (10 Gy, on a RS 2000 Biological Research X-ray Irradiator [Rad Source Technologies, Buford, GA]). Mice were monitored weekly until any criteria for euthanizing were met: severe lethargy, >10% body weight loss, or palpable hepato- or splenomegaly, in accordance with guidelines from the European Union and from the local animal ethics evaluation committee.

Intrasplenic xenograft model

NSG mice were placed on a heating pad and intraperitoneally anesthetized with a ketamine (100 mg/kg; Merial, Lyon, France) and xylazine (20 mg/kg; Bayer, Leverkusen, Germany) solution. After placing them in right lateral recumbent position, a 1-cm incision was made in the left upper abdominal wall, followed by a 1-cm incision of the peritoneum to expose the spleen. TMD8 cells (1×10^6 cells in 30 μL of phosphate-buffered saline) were gently injected into the spleen. Mice were monitored for 3 hours after surgery to ensure complete recovery.

B-cell receptor repertoire analysis

B-cell receptor repertoire analysis of unsorted splenocytes from moribund VavP-BCL2 was performed using the ImmunoSEQ assay (Adaptive Biotechnologies, Seattle, WA). Data obtained by high-throughput sequencing were analyzed with Adaptive Biotechnologies immunoSEQ analyzer proprietary software. The top 100 clones with the highest number of reads were represented as histograms, and the proportion of reads supporting the most prevalent clone among them was calculated.

Mass spectrometry analysis

Analysis was performed by the Protein Science Facility of SFR BioSciences (CNRS UAR 3444, INSERM US8, Lyon, France). Samples were reduced, alkylated, and then digested with trypsin at 37°C, overnight. They were desalted on a C18 spin column, dried, and then analyzed in triplicate using an Ultimate 3000 nano-RSLC (Thermo Fisher Scientific, San Jose, CA) coupled online with a Q-Orbitrap (Q Exactive HF; Thermo Fisher Scientific, Waltham, MA) (specific information are available in supplemental Methods).

Bimolecular fluorescence complementation

The VN-BTG1, CC-BCAR1, and CC-MDH2 constructs were cloned in the pLIX_403 vector (Addgene #41395, Watertown, MA) and were sequence verified before use. Transfection in HEK293T cells was performed with jetPRIME (Polyplus, Cat#114-15, Strasbourg, France) following the manufacturer's instructions. A total of 0.55 μg plasmid DNA was transfected per well: 150 ng plix-VN-BTG1, 150 ng plix-CC-BCAR1 or plic-CC-MDH2, and 250 ng of plix-mCherry plasmids. After 18 hours of incubation in the presence of doxycycline (100 ng/mL final), the cell-coated coverslip was taken and carefully mounted on a glass slide for image capture under confocal microscopy (LSM780, Zeiss, Oberkochen, Germany). All samples were imaged using identical settings and quantified as previously described.[29] Two biological replicates were analyzed and the BiFC signal was normalized with the mCherry signal.

Fibronectin coating and cell migration

Bovine fibronectin Reference no. F1141, Sigma-Aldrich, L'Isle d'Abeau, France) was prepared at working solutions following the manufacturer's instructions. For precoating purposes, the well plates were incubated with 40 μL of the working solution for fibronectin (final concentration of 3 μg/cm^2), collagen (100 μL/cm^2, Reference no. C2246, Sigma-Aldrich, L'Isle d'Abeau, France), and poly-L-lysine (final concentration of 0.1% in water; reference no. P4707, Sigma-Aldrich, L'Isle d'Abeau, France).

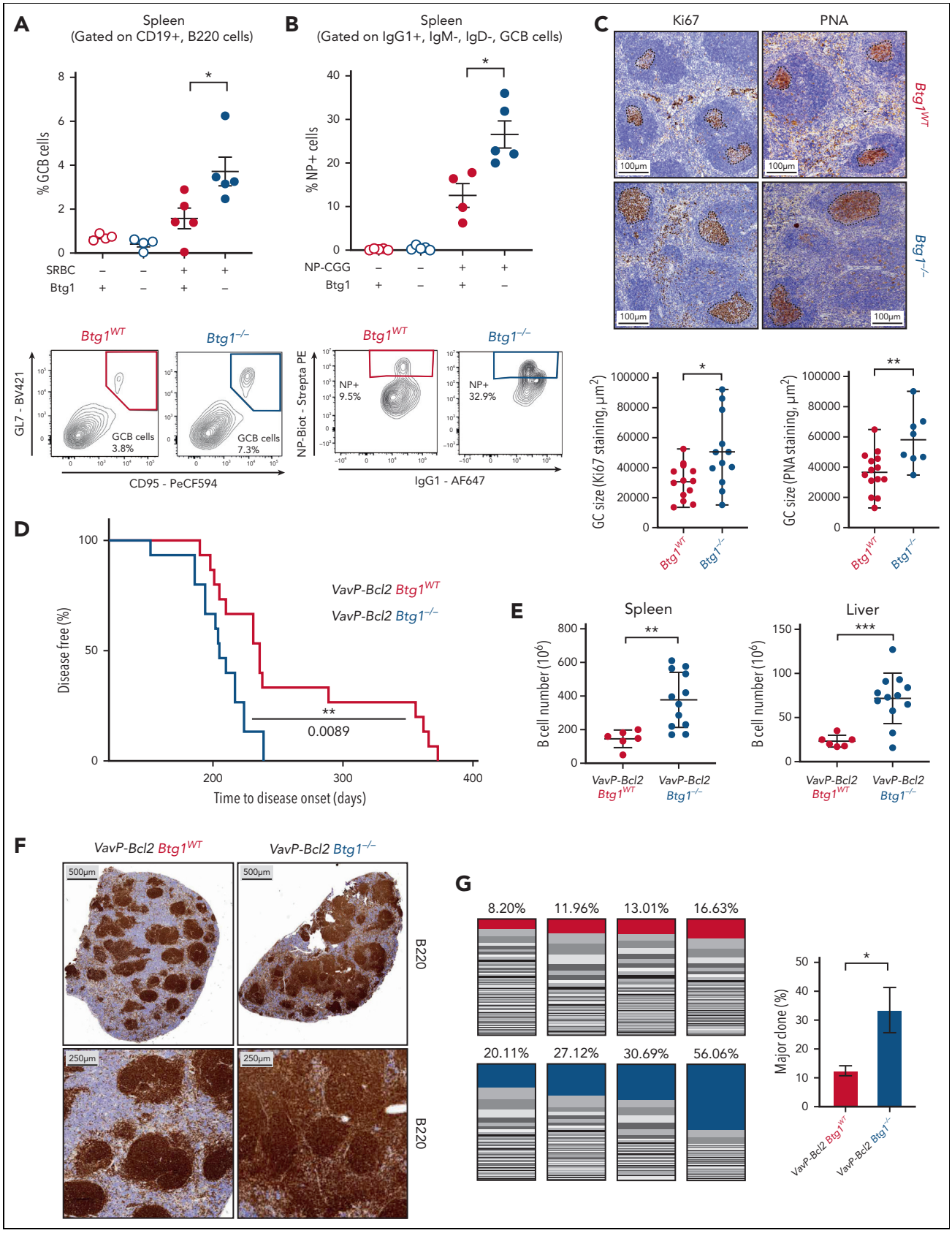

Figure 1. *Btg1* deletion is a driver of lymphomagenesis. (A-B) Flow cytometry quantification of splenic GC B cells (CD19+, B220+, CD95+, GL7+) 9 days after SRBC immunization in *Btg1*$^{-/-}$ or *Btg1*^{WT} mice. Top panel: percentage of GC B cells in the spleen of *Btg1*$^{-/-}$ or *Btg1*^{WT} mice with or without SRBC immunization (n = 4 in control group, n = 5 in SRBC-treated group). Bottom panel: example of flow cytometry histograms. (B) Flow cytometry quantification of splenic NP-CGG–specific GC B cells (CD19^{+}, B220^{+}, CD95^{+}, GL7^{+}, IgG1^{+}, IgM^{-}, IgD^{-}, NP^{+}) 9 days after NP-CGG (7) immunization in *Btg1*$^{-/-}$ or *Btg1*^{WT} mice. Top panel: percentage of NP^{+} cells in the spleen of *Btg1*$^{-/-}$

For the migration experiments, cells were seeded onto 3 μg/cm^2 fibronectin-coated wells and acquired every minute over 1 to 3 hours using an inverted microscope Zeiss Observer at 37°C. Migration speed was measured using spot detector and tracking plugin of ImageJ software (ImageJ, RRID:SCR_003070) and validated by manual counting. Experiments were performed at the BioMecan'IC facility (Institut Cochin, Paris, France).

XCelligence assays

Cell culture medium (50 μL) was added to each well of an E-Plate for impedance background measurements (Xcelligence; Agilent, Santa Clara, CA). After adding the cells and/or drugs, the final volume was 200 μL. The E-Plates were incubated at 37°C with 5% CO_2 and monitored on the real time cell analysis system every minute for 5 to 10 hours with or without treatment. When indicated, wells were coated with 3 μg/cm^2 fibronectin bovine, collagen, or poly-L-lysine.

Additional material and methods are available in supplemental Methods.

Results

BTG1 knock out is a driver of lymphomagenesis

Previous studies have shown that *Btg1* knock-out mice (*Btg1*$^{-/-}$) have a reduced number of B220-positive B-lymphocytes in the bone marrow, owing to increased apoptosis of lymphoid progenitors.[30] However, the effect of *Btg1* deletion on mature B cells remains unknown. When comparing *Btg1*$^{-/-}$ and *Btg1*^{WT} mice, no bias in the different B-cell subtypes was observed in these mice at steady state (supplemental Figure 1A). However, after intraperitoneal injection of sheep red blood cells (SRBC), a T-cell–dependent antigen, we observed GC hyperplasia in the spleen of *Btg1*$^{-/-}$ mice as compared with their WT counterparts, as revealed by an increased percentage of splenic GC B cells (GL7^{pos} and CD95^{pos}, 3.718% vs 1.578%, P = .0159, Figure 1A). Similarly, *Btg1*$^{-/-}$ mice injected with 4-hydroxy 3-nitrophényl chicken gamma globulin (NP-CGG) present higher NP-specific GC B-cell generation compared with *Btg1*^{WT} mice (26.56% vs 12.56%, P = .0159, Figure 1B). Peanut agglutinin (PNA) and Ki67 staining of spleen sections after sheep red blood cells immunization confirmed that the GCs were larger in *Btg1*$^{-/-}$ mice (mean size 58 vs 36 μm^2, P = .02, Figure 1C). These data show that *Btg1* deletion is associated with an increased GC reaction after immunization.

Next, we assessed the role of *BTG1* inactivation in lymphomagenesis. Even if *Btg1*$^{-/-}$ mice do not develop lymphoma spontaneously,[16] we hypothesized that the role of *Btg1* inactivation in lymphomagenesis might be revealed in a model driven by Bcl2 overexpression, mimicking the BCL2 amplification frequently observed in the MCD/C5 subtype of DLBCL.[8] Hence, we crossed *Btg1*$^{-/-}$ or *Btg1*^{WT} mice with VavP-Bcl2 mice and used their bone marrow to reconstitute hematopoiesis in irradiated syngeneic recipient mice (supplemental Figure 1B). As expected,[31] mice became moribund because of a lymphoproliferation associated with hepato-splenomegaly, but this occurred significantly more rapidly in mice receiving *Btg1*$^{-/-}$ bone marrow than in mice receiving *Btg1*^{WT} cells (median overall survival 205 vs 236 days, P = .0089, Figure 1D). Moreover, *Btg1*$^{-/-}$-recipient mice had a more aggressive disease, with a significant increase in the number of B cells in spleen (377 × 10^6 cells vs 145 × 10^6 cells, P = .004) and liver (72 × 10^6 cells vs 23 × 10^6 cells, P = .001) (Figure 1E). haematoxylin-eosin saffron staining and B220 immunohistochemistry staining of spleens showed lymphoid hyperplasia in all mice, which was restricted to the white pulp in the recipients of VavP-BCL2-*Btg1*^{WT} cells but infiltrated also the red pulp in the recipient of VavP-BCL2-*Btg1*$^{-/-}$ cells (Figure 1F; supplemental Figure 1C). Similarly, the perivascular and sinusoidal infiltration of the livers was more pronounced in recipients of VavP-BCL2-*Btg1*$^{-/-}$ cells compared with recipients of VavP-BCL2-*Btg1*^{WT} cells (supplemental Figure 1D). Finally, high-throughput sequencing of the genes encoding the variable region of the B-cell receptor heavy chain showed that the lymphoproliferation was more clonally restricted in *Btg1*$^{-/-}$ recipients compared with *Btg1*^{WT} recipients (Figure 1G). Altogether, these observations demonstrate that *Btg1* deletion cooperates with BCL2 overexpression to accelerate the development of an oligoclonal lymphoproliferation, which support the hypothesis that *Btg1* inactivation is a driver of lymphomagenesis.

BTG1 inactivation promotes lymphoma dissemination

Beyond its role in lymphomagenesis, and because of the enrichment of *BTG1* mutations in MCD/C5 DLBCL characterized by extranodal involvement, we hypothesized that *BTG1* deletion might also contribute to the dissemination of lymphoma cells. Hence, we developed a model of lymphoma dissemination based on intrasplenic graft in immunocompromised NSG mice of the MCD/C5-derived cell line TMD8 (harboring *MYD88* and *CD79B* mutations, but no *BTG1* mutation[26]). Mice were evaluated 5 weeks after engraftment by quantitative measurement of the lymphoma cells in the spleen and liver by flow cytometry. We used 2 different single-guide RNA targeting *BTG1* with high specificity, which did not target the closely related gene *BTG2* (supplemental Figure 2A-B). We also developed a rescue of *BTG1* (TDM8-*BTG1*^{rescue}) in the TMD8 *BTG1*$^{-/-}$ cell lines, using a lentiviral expression vector encoding the murine orthologue of *BTG1*, which is 100%

Figure 1 (continued) or *Btg1*^{WT} mice with or without NP-CGG (7) immunization (n = 5 in untreated groups, n = 4 in *Btg1*^{WT}-treated group, n = 5 in *Btg1*$^{-/-}$-treated group). Bottom panel: example of flow cytometry histograms. (C) Representative histological analysis of the spleens (top) and quantification (bottom) of SRBC-immunized *Btg1*$^{-/-}$ or *Btg1*^{WT} mice after staining with peanut agglutinin or Ki67 antibody. (D) Kaplan-Meier survival probability of irradiated mice engrafted with VavP-Bcl2-*Btg1*$^{-/-}$(blue, n = 15) and VavP-Bcl2-*Btg1*^{WT} (red, n = 15; P = .0089). (E) Absolute quantification of the number of B cells in spleen (left) and liver (right) upon sacrifice (*Btg1*^{WT}, n = 6; *Btg1*$^{-/-}$, n = 12). (F) B220 staining of representative spleen sections from VavP-Bcl2-*Btg1*$^{-/-}$ and VavP-Bcl2-*Btg1*^{WT} recipients. (G) Quantification of the clonal composition of spleens from VavP-Bcl2-*Btg1*^{WT} and VavP-Bcl2-*Btg1*$^{-/-}$ recipients (n = 4). The numbers above the histograms represent the percentage of reads corresponding to the largest clone over the 100 most represented. Right panel: comparison of the mean proportion of the major clone between VavP-BCL2-*Btg1*^{WT} and VavP-BCL2-*BTG1*$^{-/-}$ recipients (P = .0286). Values represent mean ± SEM; *P < .05; **P < .01; ***P < .001; ****P < .0001; using the Mann-Whitney test in panels A-C,E-G or log-rank (Mantel-Cox) test in panel D. ns, not significant; SEM, standard error of the mean; SRBC, sheep red blood cells.

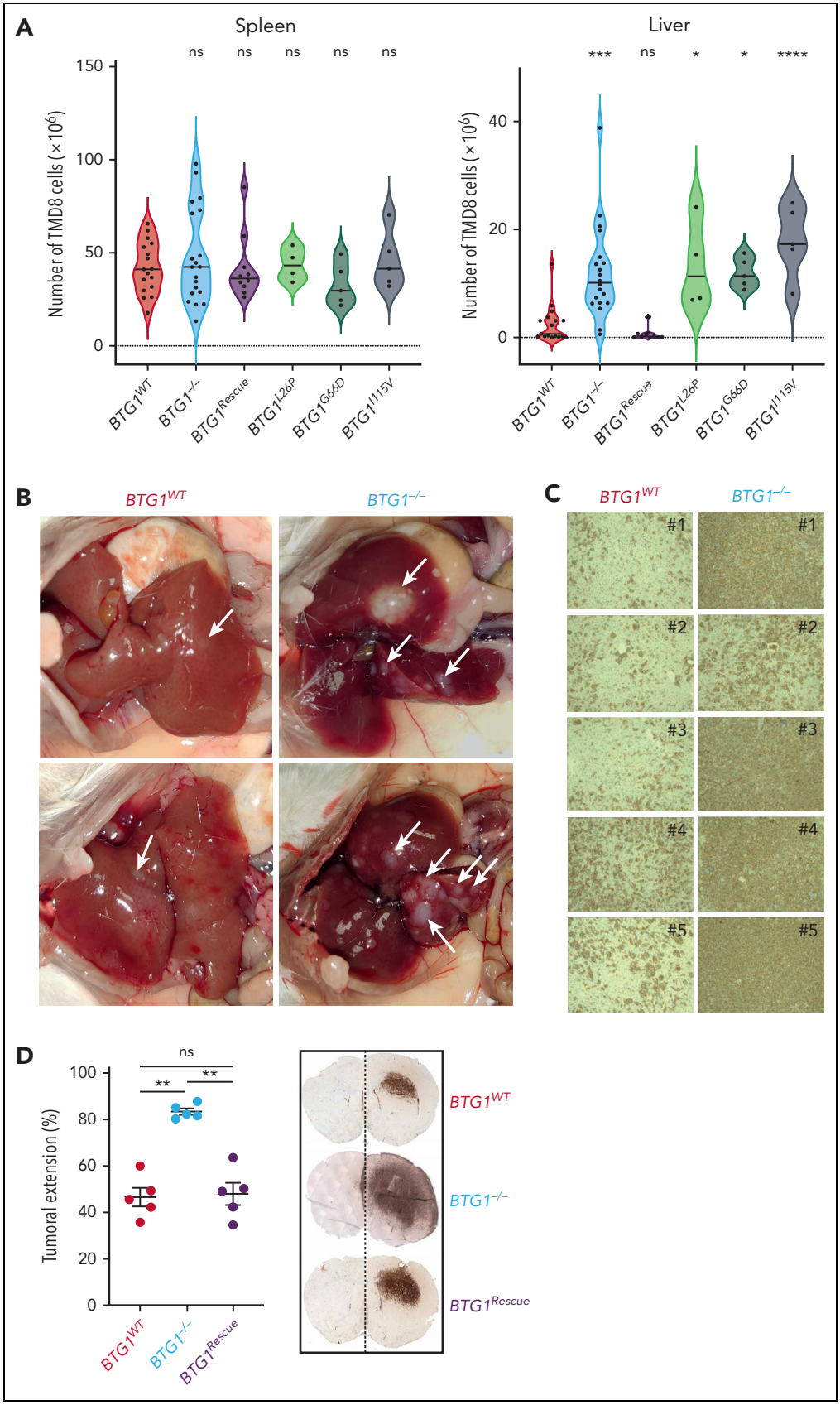

Figure 2. *BTG1* inactivation and mutations promote lymphoma dissemination. (A) Flow cytometry quantification of TMD8 cells (GFP$^+$, human CD19$^+$) in the spleen (left) and liver (right) of recipient NSG mice 5 weeks after intrasplenic xenograft (TMD8-*BTG1*^{WT}, n = 17 *BTG1*$^{-/-}$, n = 20; *BTG1*^{rescue}, n = 9; Rescue L26P, n = 4, Rescue G66D, n = 5, Rescue I1115V, n = 5). (B) Macroscopic examination and (C) immunohistochemical human CD20 staining of the liver of TMD8-*BTG1*^{WT} and TMD8-*BTG1*$^{-/-}$recipients. (D)

homologous to human BTG1 at the protein level but is not recognized by the single-guide RNA because of synonymous differences of the nucleotidic sequence (supplemental Figure 2B). Of note, BTG1 inactivation had no effect on cell proliferation or viability in vitro (supplemental Figure 2C) and did not change the sensitivity of TMD8 cells to corticosteroids, chemotherapeutic agents (doxorubicin, L-asparaginase, or methotrexate), or targeted therapies (ibrutinib or venetoclax) (supplemental Figure 2D).

Using these different TMD8 cell lines, we assessed the role of *BTG1* on lymphoma dissemination. Although *BTG1* status had no effect on the number of lymphoma cells in the spleens, there was a fivefold increase in the number of tumor cells in the livers of mice having received TMD8-*BTG1*$^{-/-}$ cells compared with those that had received TMD8-*BTG1*^{WT} cells (Figure 2A). Macroscopically, numerous tumors were noticed only in the livers of recipients of TMD8-*BTG1*$^{-/-}$ cells (Figure 2B). CD20 immunohistochemistry staining confirmed the higher number of TMD8 cells in the liver of TMD8-*BTG1*$^{-/-}$ recipients (Figure 2C). Importantly, this increased hepatic dissemination was not observed in mice having received TDM8-*BTG1*^{rescue} (Figure 2A), confirming the causal role of *BTG1* deletion in hepatic dissemination. As most *BTG1* mutations observed in patients with DLBCL are missense mutations of unknown significance, the relevance of the conclusions derived from *BTG1* knock out could be questionable. To assess this point, we rescued *BTG1*$^{-/-}$ cells with BTG1 carrying either the L26P, G66D, or I115V mutations described in patients with DLBCL. Using the in vivo dissemination assay, none of the BTG1 mutants rescued the dissemination potential of TMD8-*BTG1*$^{-/-}$ cells (Figure 2A), indicating that these missense mutations impair BTG1 functions.

TMD8 cells were not observed in the central nervous system (CNS) of the recipient mice after intrasplenic injection. However, given the frequency of CNS involvement in MCD/C5 DLBCL, we explored the consequences of *BTG1* deletion in this specific environment by using stereotaxic surgery to engraft TMD8 cells inside the brain. The dissemination of TMD8-*BTG1*$^{-/-}$ cells in the brain parenchyma was more pronounced as compared with TMD8-*BTG1*^{WT} or TDM8-*BTG1*^{rescue} cells (Figure 2D), confirming their higher dissemination ability, also within the CNS.

Effect of *BTG1* deletion on actin cytoskeleton, cell adhesion, and migration

Having established the role of *BTG1* deletion in lymphoma dissemination, we searched for the mechanism underlying this observation with the aim of finding a clinically relevant target to prevent extranodal dissemination. Given the importance of F-actin–dependent membrane extrusion in lymphoma cell migration,[32] we first analyzed the actin cytoskeleton of TMD8 cells on poly-L-lysine–coated slides, leading to unspecific cell adhesion. Phalloidin staining was diffuse in TMD8-*BTG1*^{WT} cells but showed cortical actin accumulation in TMD8-*BTG1*$^{-/-}$ cells (Figure 3A-B). After adhesion on fibronectin after integrin-mediated adhesion, confocal 3-dimensional microscopy showed that TMD8-*BTG1*$^{-/-}$ cells were flattened and presented numerous long filopodia whereas TMD8-*BTG1*^{WT} cells maintained a round shape with a reduced number of short filopodia (Figure 3C-D; supplemental Figure 3A-B). This phenotype was rescued by BTG1^{WT} (BTG1^{Rescue}) expression but not by missense BTG1 (L26P, G66D, or I115V) expression (Figure 3C-D). This phenotype was also observed in a 3-dimensional collagen matrix in which TMD8 *BTG1*$^{-/-}$ cells formed more cytoplasmic protrusions than TMD8-*BTG1*^{WT} cells (supplemental Figure 3C).

Thereafter, we quantified the cells' capacities to adhere to coated surfaces, using a Xcelligence device, to monitor the dynamics of cell adhesion processes over time. TMD8-*BTG1*$^{-/-}$ had higher adhesion capacities on fibronectin compared with TMD8-*BTG1*^{WT} (Figure 3E) whereas no difference was observed on uncoated wells or in wells coated with poly-L-lysine or collagen (supplemental Figure 3D). This was rescued by expression of BTG1^{WT} but not by missense mutant of BTG1 (supplemental Figure 3E). Finally, time-lapse microscopy demonstrated an increased motility of TMD8-*BTG1*$^{-/-}$ on fibronectin-coated surfaces compared with TMD8-*BTG1*^{WT} (20.3×10^{-2} μm.min^{-1} vs 10.3×10^{-2} μm.min^{-1}, $P < .0001$; Figure 3F; supplemental Movie 1). This was rescued by expression of BTG1^{WT} but not by missense mutant of BTG1 (Figure 3F). Altogether, these data show that *BTG1* deletion induces the redistribution of actin cytoskeleton, leading to the formation of membrane protrusions, which confer increased adhesion and migration capacities.

BCAR1 is a new BTG1 interactant

To investigate how *BTG1* deletion affects actin cytoskeleton, quantitative mass spectrometry was used to identify BTG1 interacting proteins relevant to this process. Among the 104 proteins statistically enriched after anti-hemagglutinin (HA) immunoprecipitation in cells expressing HA-tagged BTG1 compared with cells expressing HA-tagged green fluorescent protein (GFP) was BCAR1 (formerly known as p130Cas), which transduces signals after the binding of integrins to the extracellular matrix[33] (Figure 4A). After phosphorylation of its substrate domain by SRC or FAK, BCAR1 activates RAC1, which remodels actin cytoskeleton.[34] Of note, we also identified a significant enrichment of the BCAR1 partner BCAR3 in the BTG1 immunoprecipitation (supplemental Table 1). To confirm the interaction between BTG1 and BCAR1, we transfected HEK293T cells with either V5-tagged BTG1 or a control V5-tagged protein (AHCYL2). BCAR1 was found only in cells transfected by V5-tagged BTG1, and, conversely, only V5-BTG1 was immunoprecipitated with an anti-BCAR1 antibody (Figure 4B). To further confirm this interaction, we used bimolecular fluorescence complementation.[35] HEK293T cells were transfected to express the N-terminal part of the fluorescent protein Venus fused to BTG1 (VN-BTG1) and the C-terminal part of Venus fused to BCAR1 (CC-BCAR1) or to a control

Figure 2 (continued) Quantification of tumoral extension by human CD20 immunohistochemical staining of NSG mice brains after stereotaxic injection of TMD8-*BTG1*$^{-/-}$, TMD8-*BTG1*^{WT}, or TMD8-*BTG1*^{rescue} cells in the right hemisphere (n = 5) and representative images of human CD20 staining. Values represent mean or mean ± SEM; *$P < .05$; **$P < .01$; ***$P < .001$; ****$P < .0001$; using one-way ANOVA with Tukey multiple comparisons test in panel A or Mann-Whitney test in panel D. ANOVA, analysis of variance; ns, not significant; SEM, standard error of the mean.

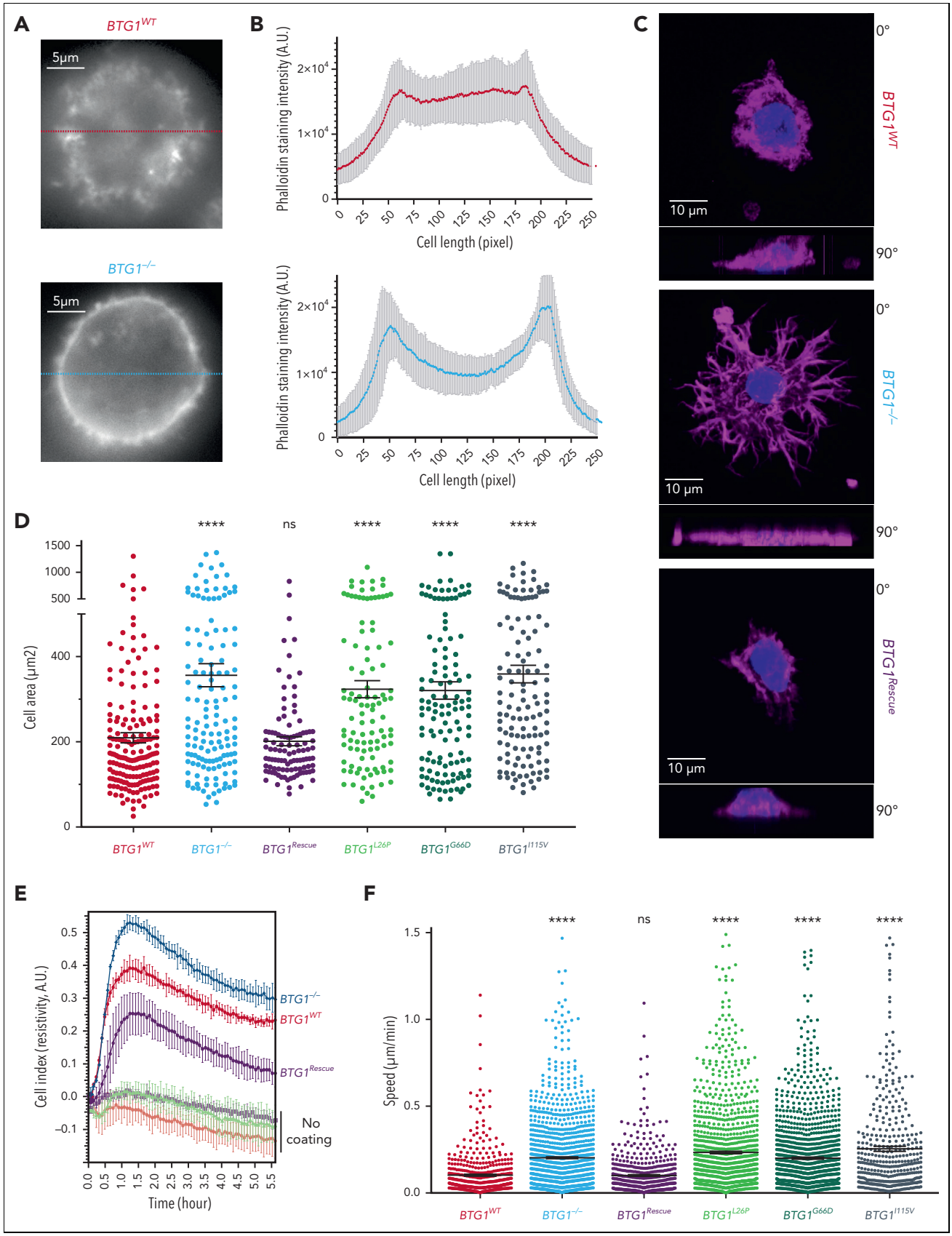

Figure 3. Effect of BTG1 deletion on actin cytoskeleton, cell adhesion, and migration. (A) Representative image and (B) quantification of phalloidin staining of TMD8-*BTG1* ^{WT} and TMD8-*BTG1*$^{-/-}$ cells on poly-L-lysine–coated slides (n = 10 for each group). (C) Confocal images in vertical (α = 0°) and horizontal (α = 90°) planes of phalloidin (purple) and Hoechst (blue) staining of TMD8-*BTG1*^{WT}, TMD8-*BTG1*$^{-/-}$, and TMD8-*BTG1*^{rescue} on fibronectin-coated slides, with (D) quantification of TMD8-*BTG1*^{WT},

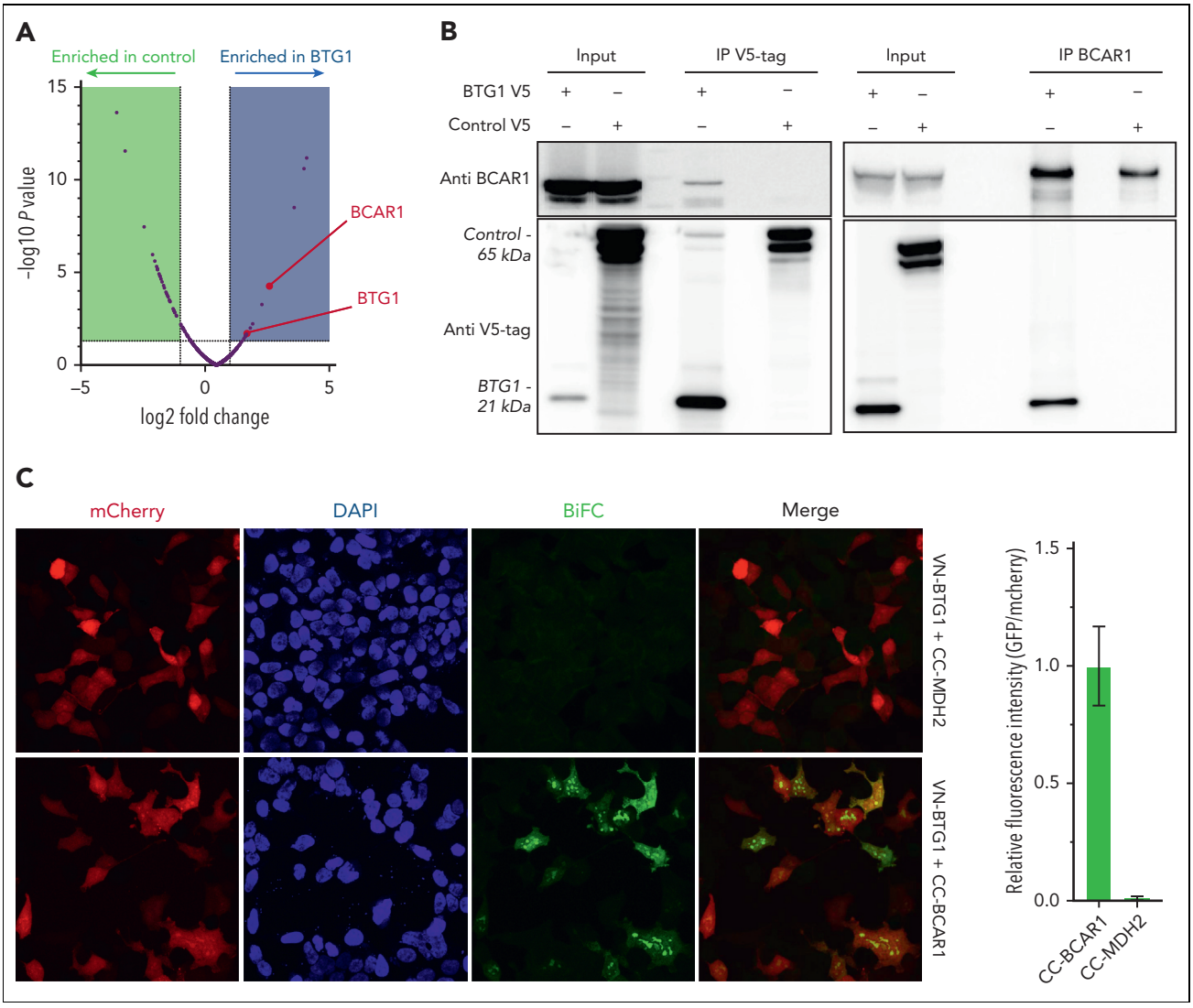

Figure 4. BCAR1 is a new BTG1 interactant. (A) Volcano plot of the proteins identified after anti-HA immunoprecipitation in cells transfected with HA-*BTG1* or HA-GFP plasmids (n = 3). (B) Coimmunoprecipitation confirmation of the BTG1-BCAR1 interaction (representative of n = 3 experiments). (C) Illustrative confocal acquisitions (original magnification ×40) (left) and quantification (right) measuring mCherry fluorescence (transfection control), DAPI (nuclear staining), and Venus fluorescence (BiFC) after transfection with VN-BTG1 and CC-MDH2 (negative control) or CC-BCAR1, as indicated (representative of 4 experiments).

protein (CC-MDH2). Despite similar levels of expression quantified with anti-VN or anti-CC GFP–coupled antibody (supplemental Figure 4), Venus fluorescence was detected only with CC-BCAR1– and VN-BTG1–transfected cells, thus confirming the interaction of BTG1 and BCAR1 (Figure 4C).

BTG1 inactivation promotes BCAR1-driven dissemination of lymphoma

Given the phenotype observed in TMD8-*BTG1*$^{-/-}$ cells, we hypothesized that BTG1 might act as an inhibitor of BCAR1. Indeed, an increased phosphorylation of BCAR1 on tyrosine 410, which attests of BCAR1 activation,[36] was observed in TMD8-*BTG1*$^{-/-}$ cells (Figure 5A), as well as in total splenocytes (supplemental Figure 5A) and sorted B lymphocytes of *Btg1*$^{-/-}$ mice (Figure 5B). We also observed in 2 other lymphoma cell lines (SUDHL-4 and OCI-LY10) that *BTG1* inactivation was associated with increased BCAR1 phosphorylation, actin cytoskeleton redistribution, increased cell area, and increased adhesion capacities on fibronectin (supplemental Figure 5B-H). The overactivation of BCAR1 was confirmed by the increased level of GTP-bound RAC1 in TMD8-*BTG1*$^{-/-}$ cells (Figure 5C). Altogether, these results show that *BTG1* deletion leads to an overactivation of the BCAR1-RAC1 pathway.

Figure 3 (continued) TMD8-*BTG1*$^{-/-}$, TMD8-*BTG1*^{rescue}, and TMD8-*BTG1*$^{rescue\ mutated}$ cell area ($P < .0001$, compared with TMD8-*BTG1*^{WT}, n = 3). (E) Cell index measurement (Xcelligence) after addition of TMD8-*BTG1*$^{-/-}$ (blue), TMD8-*BTG1*^{WT} (red), or TMD8-*BTG1*^{rescue} (purple) on fibronectin-coated or uncoated wells. (F) Quantification of cellular motility of TMD8-*BTG1*^{WT}, TMD8-*BTG1*$^{-/-}$, TMD8-*BTG1*^{rescue}, and TMD8-*BTG1*$^{rescue\ mutated}$ seeded onto fibronectin-coated slides ($P < .0001$, compared with TMD8-*BTG1*^{WT}, n = 3). Values represent mean ± SEM; ****$P < .0001$, using one-way ANOVA with Dunnett multiple comparisons test in panels D,F. ANOVA, analysis of variance; ns, not significant; SEM, standard error of the mean.

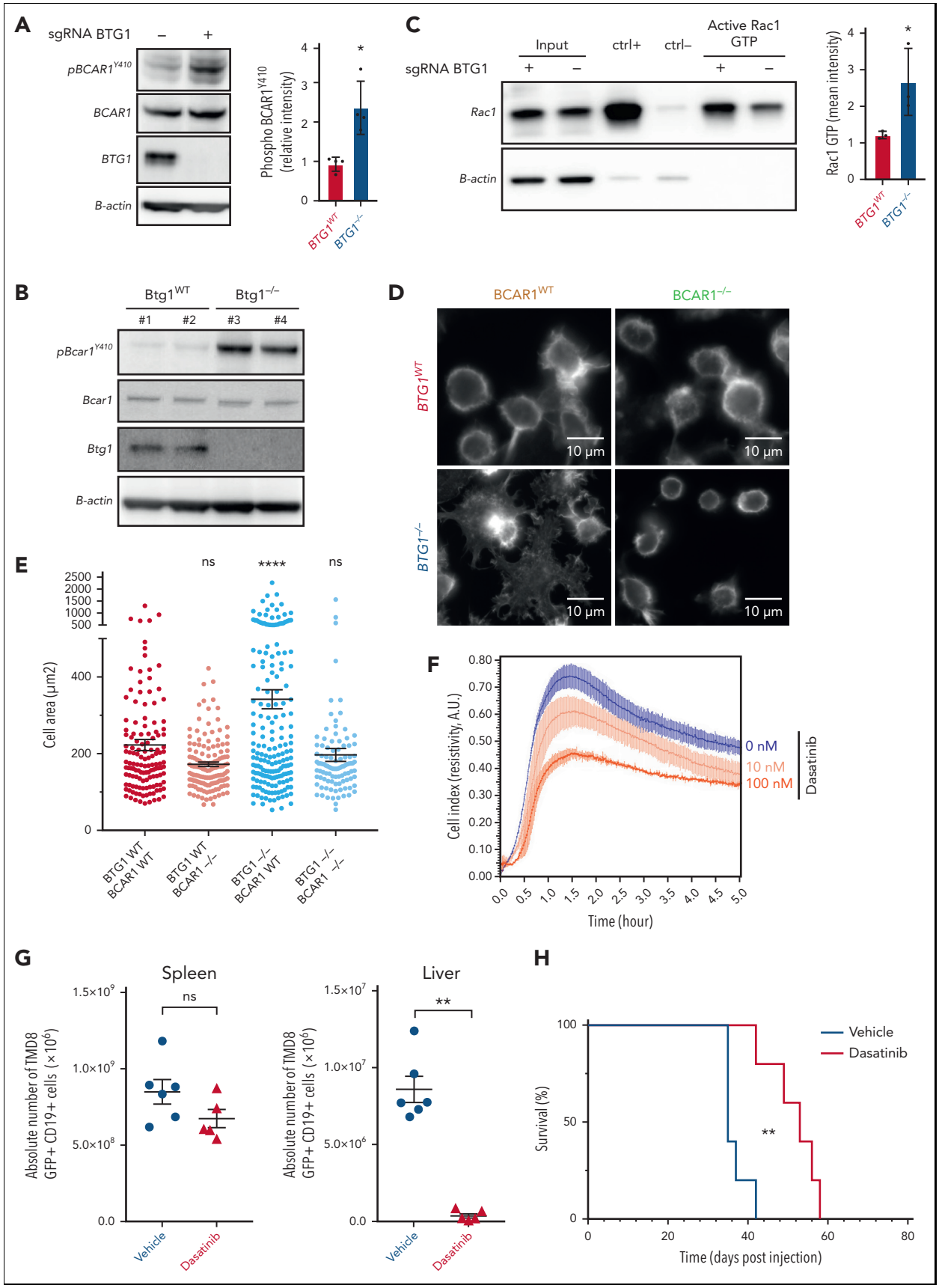

Figure 5. *BTG1* inactivation promotes BCAR1 driven dissemination of lymphoma. (A) Representative western blot and quantification of BCAR1^{Y410} phosphorylation in TMD8-*BTG1*$^{-/-}$ and TMD8-*BTG1*^{WT} cells (representative of n = 4 experiments, $P < .05$). (B) Western blot analysis of BCAR1^{Y410} phosphorylation of sorted splenic B

The functional role of the BCAR1-RAC1 pathway in the dissemination phenotype of TMD8-*BTG1*$^{-/-}$ cells was further investigated with genetic and pharmacologic inhibition of this pathway. Using CRISPR/Cas9, we knocked out *BCAR1* in TMD8-*BTG1*$^{-/-}$ cells (supplemental Figure 6A) and we observed a complete rescue of the adhesion phenotype conferred by *BTG1* inactivation (Figure 5D-E; supplemental Figure 6B). Then, we used dasatinib to inhibit the phosphorylation of BCAR1 by SRC. As expected, SRC inhibition reduced the phosphorylation of BCAR1 and the level of RAC1-GTP (supplemental Figure 6C-D). Accordingly, short-term (2 hours) exposure to dasatinib strongly impaired the ability of TMD8-*BTG1*$^{-/-}$ cells to adhere to fibronectin (Figure 5D) without any detectable effect on cell survival (supplemental Figure 6E). Of note, even a low dose (10 nM), which did not induce cell death after long-term exposure (72 hours) (supplemental Figure 6F), had a significant effect on cell adhesion capacities. To confirm the relevance of this observation in vivo, we analyzed the effect of dasatinib treatment on hepatic dissemination after intrasplenic engraftment. Whereas dasatinib treatment had no effect on the proliferation of TMD8-*BTG1*$^{-/-}$ cells in the spleen, it dramatically decreased hepatic dissemination (Figure 5G; supplemental Figure 6G) and significantly increased the survival of mice compared with mice treated with excipient (median survival 35 days vs 53 days, $P = .0041$, Figure 5H). Thus confirming, in vivo, that SRC inhibition can prevent lymphoma dissemination driven by the BCAR1-RAC1 pathway after *BTG1* inactivation.

Discussion

Following the extensive characterization of the genomic landscape of cancers, the driver/passenger dichotomy has been widely used to prioritize the recurrently mutated genes for further functional analyses. However, this classification relies on algorithmic analysis of genomic data, which produce highly variable results.[37] In B-cell neoplasms, the genes harboring a strong signature of the activity of activation-induced cytidine deaminase, such as *BTG1*, have mostly been considered as passengers of lymphomagenesis.[8] However, the data presented here support the hypothesis that *BTG1* mutations are actively driving the process of lymphomagenesis. First, we observed that *BTG1* inactivation increases the magnitude of the GC reaction after immunization by a T-cell–dependent antigen, suggesting important functions of this gene in the physiology of mature B cells. Second, by using a classical model of Bcl2 overexpression, we observed that *Btg1* deletion accelerated the development of an oligoclonal lymphoproliferation, as was previously shown for other drivers of lymphomagenesis such as *CREBBP*,[38] *KMT2D*,[39] or *TBL1XR1*.[11] The data presented here do not formally demonstrate that *BTG1* inactivation drives lymphomagenesis in a cell-intrinsic manner, and we cannot exclude that the inactivation of *BTG1* in other hematopoietic cells have contributed to the observed phenotype. Of note, Mlynarczyk and Melnick[40] have observed a similar acceleration of VavP-BCL2 lymphoproliferation after expression of a BTG1 missense mutation (Q36H) restricted to B cells, which strongly support the cell-intrinsic role of BTG1 in lymphomagenesis. Third, we observed that all the missense mutations tested phenocopied the dissemination phenotype observed after *BTG1* deletion, suggesting that the conclusions derived from genetic knock out of *BTG1* are applicable not only to patients with false sense mutations, but also to patients with missense mutations. This is in accordance with a recently published report assessing in vitro the effects of *BTG1* missense mutations on its ability to interact with the CCR4-Not complex, which also concluded that most of the missense mutations were loss-of-function mutations.[41] Finally, it is not common to observe multiple *BTG1* mutations in cis (on the same allele) in DLBCL (5% of DLBCL, according to[42]) probably as a result of activation-induced cytidine deaminase activity, which also supports the hypothesis that BTG1 activity is impaired in mutated DLBCL.

The data presented here also demonstrate that *BTG1* inactivation has a strong effect on lymphoma dissemination. Extranodal dissemination has long been recognized as a poor prognostic factor included into the International Prognostic Index,[43] but the molecular mechanisms explaining the outspread of lymphoma cells outside of the lymph nodes have not been studied extensively. Interestingly, overexpression of BCAR1 was already noted in a model of CNS involvement after intravenous injection of a lymphoma cell line.[44] Our study reveals another mechanism of BCAR1 overactivation, after the loss of the inhibitory interaction between BTG1 and BCAR1. The release of this interaction provokes major changes of the actin cytoskeleton leading to the formation of numerous filopodia, associated with increased adhesion and spreading on fibronectin and increased in vitro migration, supporting the increased migration capacities in vivo. Of note, BCAR1 activity also contributes to the sensing of the mechanical properties of the extracellular matrix[45] and the metastatic spreading of breast cancers,[46,47] suggesting a broader role of this pathway in cancer. Accordingly, therapeutic targeting of the BCAR1-RAC1 pathway is an interesting avenue, which can be achieved indirectly by SRC inhibitors such as dasatinib.

Dasatinib has already been studied in preclinical models of DLBCL, showing cytotoxic activity against cell lines in vitro and in vivo, mostly owing to FYN inhibition.[48] However, the efficacy of dasatinib as a cytotoxic agent in DLBCL was not confirmed in a phase 1-2 trial of dasatinib in relapsed or refractory non-Hodgkin lymphomas including 8 patients with DLBCL.[49] The experimental results described here suggest that dasatinib might be an interesting drug in DLBCL beyond its cytotoxic

Figure 5 (continued) lymphocytes from *Btg1*^{WT} or *Btg1*$^{-/-}$ mice (n = 2 per group). (C) Immunoprecipitation (representative of n = 3 experiments) and quantification of RAC1-GTP in TMD8-*BTG1*$^{-/-}$ and TMD8-*BTG1*^{WT} cells ($P < .05$). (D) Representative confocal images of phalloidin staining and (E) quantification of TMD8-*BTG1*^{WT}-*BCAR1*$^{-/-}$, TMD8-*BTG1*$^{-/-}$-*BCAR1*^{WT}, and TMD8-*BTG1*$^{-/-}$-*BCAR1*$^{-/-}$ cell area on fibronectin-coated slides ($P < .0001$ compared with TMD8-*BTG1*^{WT}-*BCAR1*^{WT}). (F) Resistivity measurement estimated by the cell index (Xcelligence) of TMD8-*BTG1*$^{-/-}$ cells on fibronectin-coated wells after dasatinib pretreatment (excipient, 0.01 and 0.1 μM for 30 minutes). (G) Flow cytometry quantification of TMD8-*BTG1*$^{-/-}$ cells in the spleen and liver of recipient NSG mice treated by 5 daily injections of dasatinib (n = 5) or vehicle (n = 6), ($P < .01$ compared with vehicle). (H) Kaplan-Meier survival probability of NSG mice after intrasplenic injection of TMD8-*BTG1*$^{-/-}$ cells and treatment with vehicle (blue, n = 5) or dasatinib (orange, n = 5; $^{**}P = .0041$). Values represent mean ± SEM; $^{*}P < .05$; $^{**}P < .01$; $^{****}P < .0001$; using the Mann-Whitney test in panels A,C,G, one-way ANOVA with Dunnett multiple comparisons test in panel E, and log-rank test in panel H. ANOVA, analysis of variance; ns, not significant; SEM, standard error of the mean.

activity, by inhibiting the BCAR1-RAC1–mediated dissemination. Accordingly, dasatinib could be repurposed to prevent extranodal relapse of *BTG1*-mutated DLBCL, and this strategy might be evaluated in clinical trials.

In conclusion, we provide evidence that *BTG1* mutations actively contribute to lymphomagenesis, GCs reaction, and cellular dissemination by modulation of BCAR1-RAC1 pathway.

Acknowledgments

The authors thank Adeline Page and Frédéric Delolme for performing the mass spectrometry analysis (Protein Science Facility, SFR Biosciences CNRS UAR3444, Inserm US8, UCBL, ENS de Lyon) and the staff of the Central Unit for Electron Microscopy at DKFZ for technical support. In addition, the authors thank Charlotte Lamirault and Mathieu Maurin for carrying out the intracerebral xenograft experiment (Institut Curie, Site de Saint-Cloud, Hematologie, et INSERM U932 Institut Curie, PSL Research University, Paris, France). The authors acknowledge the contribution of the AniRA lentivector production facility from the CELPHEDIA Infrastructure and SFR Biosciences (UAR 3444/CNRS, US8/Inserm, ENS de Lyon, UCBL), especially Gisèle Froment, Didier Nègre, and Caroline Costa; and thank Yunlong Jia (IGFL, CNRS, Team Ontogenesis and Molecular Interactions) for his help on BiFC tuning. Furthermore, the authors thank Sandrine Roulland, Jean-Jacques Diaz, and Ari Melnick for helpful discussions; and Verena Landel from Hospices Civils de Lyon for English editing.

This work was supported by grants from the L'Association pour la Recherche sur le Cancer, La Ligue contre le Cancer, Lyrican (INCA DGOS INSERM_12563 grant), and the Hospices Civils de Lyon.

Authorship

Contribution: L.D., L.G., J.-P.R., and P.S. conceptualized the study and acquired funding; L.D., M.L., C.K., E. Bardel, A.C., D.C., A.-L.P., L.G., P.A., A.J., S.D., S.M., and J.-P.R. performed the investigations; L.D., O.D., P.A., H.-J.D., G.S., L.G., J.-P.R., and P.S. designed the methodology; C.S., A.T.-G., E. Bachy, H.G., H.-J.D., S.M., and P.A. provided resources; L.G, J.-P.R., and P.S. supervised the study; and L.D., L.G., M.B., J.-P.R., and P.S. wrote the original draft.

Conflict-of-interest disclosure: The authors declare no competing financial interests.

ORCID profiles: L.D., 0000-0002-3838-8763; C.K., 0000-0001-9398-7200; P.A., 0000-0002-2481-8275; S.M., 0000-0001-7629-703X; G.S., 0000-0002-9541-8666; E. Bachy, 0000-0003-2694-7510; P.S., 0000-0003-1724-4792.

Correspondence: Jean-Pierre Rouault, Equipe LIB, faculté de médecine Lyon-Sud, 165 chemin du Grand Revoyet, BP12, 69921 Oullins Cedex, France; email: jean-pierre.rouault@univ-lyon1.fr; and Pierre Sujobert, Hospices Civils de Lyon, Laboratoire d'Hématologie, 165 chemin du Grand Revoyet, 69495 Pierre Benite Cedex, France; email: pierre.sujobert@chu-lyon.fr.

Footnotes

Submitted 4 May 2022; accepted 1 November 2022; prepublished online on *Blood* First Edition 14 November 2022. https://doi.org/10.1182/blood.2022016943.

*J.-P.R. and P.S. contributed equally to this study.

Data are available on request from the corresponding author, Pierre Sujobert (pierre.sujobert@chu-lyon.fr) or Jean-Pierre Rouault (jean-pierre.rouault@univ-lyon1.fr)

The online version of this article contains a data supplement.

The publication costs of this article were defrayed in part by page charge payment. Therefore, and solely to indicate this fact, this article is hereby marked "advertisement" in accordance with 18 USC section 1734.

REFERENCES

1. Sehn LH, Salles G. Diffuse large B-cell lymphoma. *N Engl J Med*. 2021;384(9):842-858.
2. Alizadeh AA, Elsen MB, Davis RE, et al. Distinct types of diffuse large B-cell lymphoma identified by gene expression profiling. *Nature*. 2000;403(6769):503-511.
3. Davis RE, Ngo VN, Lenz G, et al. Chronic active B-cell-receptor signalling in diffuse large B-cell lymphoma. *Nature*. 2010;463(7277):88-92.
4. Yang Y, Shaffer AL, Emre NCT, et al. Exploiting synthetic lethality for the therapy of ABC diffuse large B cell lymphoma. *Cancer Cell*. 2012;21(6):723-737.
5. Davies A, Cummin TE, Barrans S, et al. Gene-expression profiling of bortezomib added to standard chemoimmunotherapy for diffuse large B-cell lymphoma (REMoDL-B): an open-label, randomised, phase 3 trial. *Lancet Oncol*. 2019;20(5):649-662.
6. Younes A, Sehn LH, Johnson P, et al. Randomized phase III trial of ibrutinib and rituximab plus cyclophosphamide, doxorubicin, vincristine, and prednisone in non–germinal center B-cell diffuse large B-cell lymphoma. *J Clin Oncol*. 2019;37(15):1285-1295.
7. Nowakowski GS, Hong F, Scott DW, et al. Addition of lenalidomide to R-CHOP improves outcomes in newly diagnosed diffuse large B-cell lymphoma in a randomized phase II US Intergroup Study ECOG-ACRIN E1412. *J Clin Oncol*. 2021;39(12):1329-1338.
8. Chapuy B, Stewart C, Dunford AJ, et al. Molecular subtypes of diffuse large B cell lymphoma are associated with distinct pathogenic mechanisms and outcomes. *Nat Med*. 2018;24(5):679-690.
9. Schmitz R, Wright GW, Huang DW, et al. Genetics and pathogenesis of diffuse large B-cell lymphoma. *N Engl J Med*. 2018;378(15):1396-1407.
10. Wright GW, Huang DW, Phelan JD, et al. A probabilistic classification tool for genetic subtypes of diffuse large B cell lymphoma with therapeutic implications. *Cancer Cell*. 2020;37(4):551-568.e14.
11. Venturutti L, Teater M, Zhai A, et al. TBL1XR1 mutations drive extranodal lymphoma by inducing a pro-tumorigenic memory fate. *Cell*. 2020;182(2):297-316.e27.
12. Matsuda S, Rouault J-P, Magaud J-P, Berthet C. In search of a function for the TIS21 / PC3 / BTG1 / TOB family. *FEBS Lett*. 2001;497(2–3):67-72.
13. Rouault JP, Rimokh R, Tessa C, et al. BTG1, a member of a new family of antiproliferative genes. *EMBO J*. 1992;11(4):1663-1670.
14. Yuniati L, Scheijen B, van der Meer LT, van Leeuwen FN. Tumor suppressors BTG1 and BTG2: beyond growth control. *J Cell Physiol*. 2019;234(5):5379-5389.
15. Winkler GS. The mammalian anti-proliferative BTG/Tob protein family. *J Cell Physiol*. 2010;222(1):66-72.
16. Scheijen B, Boer JM, Marke R, et al. Tumor suppressors BTG1 and IKZF1 cooperate during mouse leukemia development and increase relapse risk in B-cell precursor acute lymphoblastic leukemia patients. *Haematologica*. 2017;102(3):541-551.
17. Waanders E, Scheijen B, van der Meer LT, et al. The origin and nature of tightly clustered BTG1 deletions in precursor B-cell acute lymphoblastic leukemia support a model of multiclonal evolution. *PLoS Genet*. 2012;8(2):e1002533.
18. Rouault JP, Prévôt D, Berthet C, et al. Interaction of BTG1 and p53-regulated BTG2 gene products with mCaf1, the murine homolog of a component of the yeast CCR4 transcriptional regulatory complex. *J Biol Chem*. 1998;273(35):22563-22569.

19. Mauxion F, Chen CYA, Séraphin B, Shyu A Bin. BTG/TOB factors impact deadenylases. *Trends Biochem Sci*. 2009;34(12):640-647.

20. Berthet C, Guéhenneux F, Revol V, et al. Interaction of PRMT1 with BTG/TOB proteins in cell signalling: molecular analysis and functional aspects. *Genes Cells*. 2002;7(1):29-39.

21. Lin WJ, Gary JD, Yang MC, Clarke S, Herschman HR. The mammalian immediate-early TIS21 protein and the leukemia-associated BTG1 protein interact with a protein-arginine N-methyltransferase. *J Biol Chem*. 1996;271(25):15034-15044.

22. Duke JL, Liu M, Yaari G, et al. Multiple transcription factor binding sites predict AID targeting in non-Ig genes. *J Immunol*. 2013;190(8):3878-3888.

23. Amin AD, Peters TL, Li L, et al. Diffuse large B-cell lymphoma: can genomics improve treatment options for a curable cancer? *Cold Spring Harb Mol Case Stud*. 2017;3(3):a001719.

24. Reddy A, Zhang J, Davis NS, et al. Genetic and functional drivers of diffuse large B cell lymphoma. *Cell*. 2017;171(2):481-494.e15.

25. Xia M, David L, Teater M, et al. BCL10 mutations define distinct dependencies guiding precision therapy for DLBCL. *Cancer Discov*. 2022;12(8):1922-1941.

26. Tohda S, Sato T, Kogoshi H, et al. Establishment of a novel B-cell lymphoma cell line with suppressed growth by gamma-secretase inhibitors. *Leuk Res*. 2006;30(11):1385-1390.

27. Ogilvy S, Metcalf D, Print CG, et al. Constitutive Bcl-2 expression throughout the hematopoietic compartment affects multiple lineages and enhances progenitor cell survival. *Proc Natl Acad Sci U S A*. 1999;96(26):14943-14948.

28. Farioli-Vecchioli S, Micheli L, Saraulli D, et al. Btg1 is required to maintain the pool of stem and progenitor cells of the dentate gyrus and subventricular zone. *Front Neurosci*. 2012;6:124.

29. Dard A, Reboulet J, Jia Y, et al. Human HOX proteins use diverse and context-dependent motifs to interact with TALE class cofactors. *Cell Rep*. 2018;22(11):3058-3071.

30. Tijchon E, van Emst L, Yuniati L, et al. Tumor suppressors BTG1 and BTG2 regulate early mouse B-cell development. *Haematologica*. 2016;101(7):e272-e276.

31. Egle A, Harris AW, Bath ML, et al. VavP-Bcl2 transgenic mice develop follicular lymphoma preceded by germinal center hyperplasia. *Blood*. 2004;103(6):2276-2283.

32. Jacquemet G, Hamidi H, Ivaska J. Filopodia in cell adhesion, 3D migration and cancer cell invasion. *Curr Opin Cell Biol*. 2015;36:23-31.

33. Sun G, Cheng SYS, Chen M, Lim CJ, Pallen CJ. Protein tyrosine phosphatase α phosphotyrosyl-789 binds BCAR3 to position Cas for activation at integrin-mediated focal adhesions. *Mol Cell Biol*. 2012;32(18):3776-3789.

34. Sharma A, Mayer BJ. Phosphorylation of p130Cas initiates Rac activation and membrane ruffling. *BMC Cell Biol*. 2008;9(50):1-15.

35. Hu CD, Kerppola TK. Simultaneous visualization of multiple protein interactions in living cells using multicolor fluorescence complementation analysis. *Nat Biotechnol*. 2003;21(5):539-545.

36. Jacquemet G, Stubb A, Saup R, et al. Filopodome mapping identifies p130Cas as a mechanosensitive regulator of filopodia stability. *Curr Biol*. 2019;29(2):202-216.e7.

37. Tokheim CJ, Papadopoulos N, Kinzler KW, Vogelstein B, Karchin R. Evaluating the evaluation of cancer driver genes. *Proc Natl Acad Sci U S A*. 2016;113(50):14330-14335.

38. Pasqualucci L, Dominguez-Sola D, Chiarenza A, et al. Inactivating mutations of acetyltransferase genes in B-cell lymphoma. *Nature*. 2011;471(7337):189-196.

39. Ortega-Molina A, Boss IW, Canela A, et al. The histone lysine methyltransferase KMT2D sustains a gene expression program that represses B cell lymphoma development. *Nat Med*. 2015;21(10):1199-1208.

40. Mlynarczyk C, Melnick A. BTG1 mutation is associated with aggressive lymphomagenesis in human and animal models of diffuse large B-cell lymphoma. *Blood*. 2021;138(supplement 1):359.

41. Almasmoum HA, Airhihen B, Seedhouse C, Winkler GS. Frequent loss of BTG1 activity and impaired interactions with the Caf1 subunit of the Ccr4–not deadenylase in non-Hodgkin lymphoma. *Leuk Lymphoma*. 2021;62(2):281-290.

42. Kurtz DM, Soo J, Co Ting Keh L, et al. Enhanced detection of minimal residual disease by targeted sequencing of phased variants in circulating tumor DNA. *Nat Biotechnol*. 2021;39(12):1537-1547.

43. Shipp MA, Harrington PD, Anderson JR, et al. The International Non-Hodgkin's Lymphoma Project, a predictive model for aggressiv non-Hodgkin's lymphoma. *N Engl J Med*. 1993;329(14):987-994.

44. Bosch R, Moreno MJ, Dieguez-Gonzalez R, et al. A novel orally available inhibitor of focal adhesion signaling increases survival in a xenograft model of diffuse large B-cell lymphoma with central nervous system involvement. *Haematologica*. 2013;98(8):1242-1249.

45. Matsui H, Harada I, Sawada Y. Src, p130Cas, and mechanotransduction in cancer cells. *Genes Cancer*. 2012;3(5-6):394-401.

46. Cabodi S, Del Pilar Camacho-Leal M, Di Stefano P, Defilippi P. Integrin signalling adaptors: not only figurants in the cancer story. *Nat Rev Cancer*. 2010;10(12):858-870.

47. Cabodi S, Tinnirello A, Bisaro B, et al. p130Cas is an essential transducer element in ErbB2 transformation. *FASEB J*. 2010;24(10):3796-3808.

48. Scuoppo C, Wang J, Persaud M, et al. Repurposing dasatinib for diffuse large B cell lymphoma. *Proc Natl Acad Sci U S A*. 2019;116(34):16981-16986.

49. Umakanthan JM, Iqbal J, Batlevi CL, et al. Phase I/II study of dasatinib and exploratory genomic analysis in relapsed or refractory non-Hodgkin lymphoma. *Br J Haematol*. 2019;184(5):744-752.